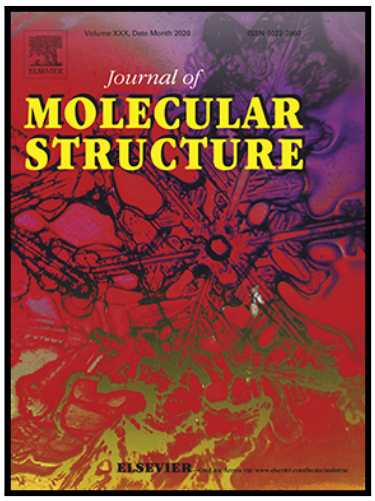

Framework robustness in early d-block metal complexes with tripodal polyalcohol ligands

Carla Krupczak , Bruno J. Stoeberl , Kátia C.M. Westrup , Lorenzo Tesi , Francielli S. Santana , Siddhartha O.K. Giese , Fabiano Yokaichiya , Daniel da S. Costa , Juliana M. Missina , Danilo Stinghen , David L. Hughes , Roberta Sessoli , Giovana G. Nunes , Dayane M. Reis , Jaísa F. Soares

PII: S0022-2860(22)02009-9
DOI: https://doi.org/10.1016/j.molstruc.2022.134360
Reference: MOLSTR 134360

To appear in: *Journal of Molecular Structure*

Received date: 15 August 2022
Revised date: 11 October 2022
Accepted date: 16 October 2022

Please cite this article as: Carla Krupczak , Bruno J. Stoeberl , Kátia C.M. Westrup , Lorenzo Tesi , Francielli S. Santana , Siddhartha O.K. Giese , Fabiano Yokaichiya , Daniel da S. Costa , Juliana M. Missina , Danilo Stinghen , David L. Hughes , Roberta Sessoli , Giovana G. Nunes , Dayane M. Reis , Jaísa F. Soares , Framework robustness in early d-block metal complexes with tripodal polyalcohol ligands, *Journal of Molecular Structure* (2022), doi: https://doi.org/10.1016/j.molstruc.2022.134360

Highlights

- Tripodal alcohols provide versatile coordination modes for transition metal ions.
- Spontaneous polyalcohol deprotonation leads to binuclear M^{III} complexes.
- The versatile tripodal ligands confer notable robustness to the binuclear aggregates.
- Products are formed in air or inert atmosphere and non-protic or protic media.
- Metal ion oxidation or solvent loss does not lead to product decomposition.

Framework robustness in early d-block metal complexes with tripodal polyalcohol ligands

Carla Krupczak[a,♦], Bruno J. Stoeberl[b,♦], Kátia C. M. Westrup[a,♦], Lorenzo Tesi[c,d], Francielli S. Santana[a], Siddhartha O. K. Giese[a], Fabiano Yokaichiya[e], Daniel da S. Costa[e], Juliana M. Missina[a], Danilo Stinghen[a], David L. Hughes[f], Roberta Sessoli[c], Giovana G. Nunes[a], Dayane M. Reis[b,*], Jaísa F. Soares[a,*]

[a] *Department of Chemistry, Federal University of Parana, Centro Politecnico, Jardim das Americas, 81531-980 Curitiba, PR, Brazil*

[b] *Department of Chemistry and Biology, Federal University of Technology – Parana, Cidade Industrial, 81280-340 Curitiba, PR, Brazil*

[c] *Department of Chemistry "U. Schiff" and INSTM UdR Firenze, University of Florence, Via della Lastruccia 3-13, 50019 Sesto Fiorentino, FI, Italy*

[d] *Institute of Physical Chemistry, University of Stuttgart, Pfaffenwaldring 55, 70569 Stuttgart, Germany*

[e] *Department of Physics, Federal University of Parana, Centro Politecnico, Jardim das Americas, 81531-980 Curitiba, PR, Brazil*

[f] *School of Chemistry, University of East Anglia, Norwich NR4 7TJ, United Kingdom*

♦ These authors contributed equally.

Corresponding authors

Jaísa F. Soares – jaisa.soares@ufpr.br

Dayane M. Reis – dayane@utfpr.edu.br

Graphical abstract

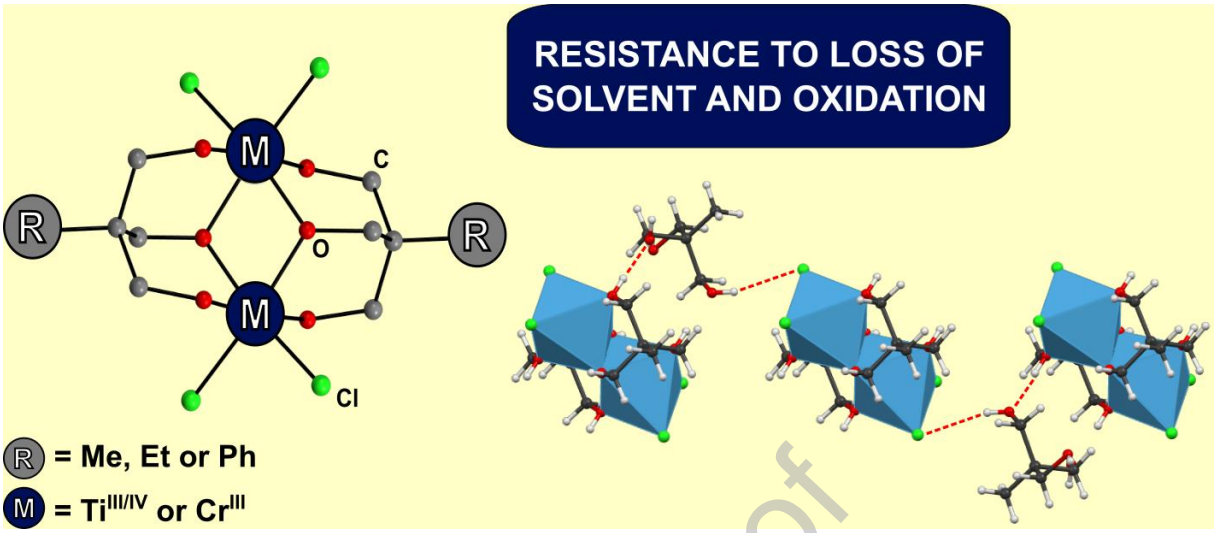

ABSTRACT

While performing our research on the tetranuclear "star-shaped" complexes formulated as $[M_3M'(L^R)_2(dpm)_6]$, where M, M' are first-row *d*-block metals; H_3L^R is a tripodal alcohol, $RC(CH_2OH)_3$, with R = Et, Me or Ph; and Hdpm = dipivaloylmethane, we isolated a series of binuclear, alkoxide-bridged chelate complexes of titanium and chromium upon spontaneous deprotonation of the polyalcohol. In the titanium system, both $[Ti^{III}_2Cl_4(H_2L^{Et})_2]\cdot 4thf$ and $[Ti^{IV}_2Cl_4(HL^{Et})_2]\cdot 2thf$ were identified; they present analogous binuclear frameworks but distinct metal oxidation states and polyalcohol deprotonation degrees. Four similar Cr^{III}_2 compounds were also isolated, differing in the tripodal R groups and cocrystallized solvent or proligand molecules. The products were characterized by single-crystal X-ray diffraction analysis and spectroscopic, thermogravimetric and magnetic measurements. Cocrystallization influences the nature, strength and pattern of intermolecular interactions. Among the binuclear M^{III} products, all those containing solvating tetrahydrofuran, $[M_2Cl_4(H_2L^R)_2]\cdot x$ thf (R = Et, Ph; *x* = 4 or 5 respectively), lose solvent upon gradual polyalcohol deprotonation, mild heating or vacuum drying. The versatile tripodal skeleton assembles the alkoxide-bridged M_2 units (M =

$Ti^{III/IV}$ or Cr^{III}) in various experimental conditions, including air or inert atmosphere and non-protic or protic media, and confers remarkable robustness to the final binuclear aggregates.

Keywords

Binuclear; tripodal; polyalcohol; spontaneous deprotonation; early transition metal; intermolecular interactions

1. Introduction

"Star-shaped" metal complexes have attracted attention since the first report of the single-molecule magnet (SMM) behavior of $[Fe_4(\mu\text{-}OMe)_6(dpm)_6]$, Hdpm = dipivaloylmethane, commonly referred to as **Fe_4** [1]. The structure of this complex presents a central iron(III) ion, which is antiferromagnetically coupled to other three (peripheral) iron(III) centers, giving rise to a non-compensated total spin state with *S* = 5 (Scheme 1a). Subsequent studies demonstrated that the replacement of the methoxide bridges by chelating tripodal alkoxides, $RC(CH_2O^-)_3$ (abbreviated $(L^R)^{3-}$, with R = Me, Ph, CH_2Br and Bu^t, Scheme 1b-c)[1] stabilizes further the tetranuclear structure and increases the magnetic anisotropy barrier [2-4]. Moreover, the proper choice of R groups makes it possible to adsorb the complexes on surfaces without significant loss of their magnetic memory [5, 6], which is vital for the integration of SMMs in devices.

[1] The H_3L^R abbreviation for the tripodal alcohols emphasizes the three ionizable hydroxyl H atoms, while R represents the alkyl or aryl group bound to the polyalcohol's bridgehead carbon. The letter "L" replaces the tripodal alcohol skeleton as depicted in Scheme 1c.

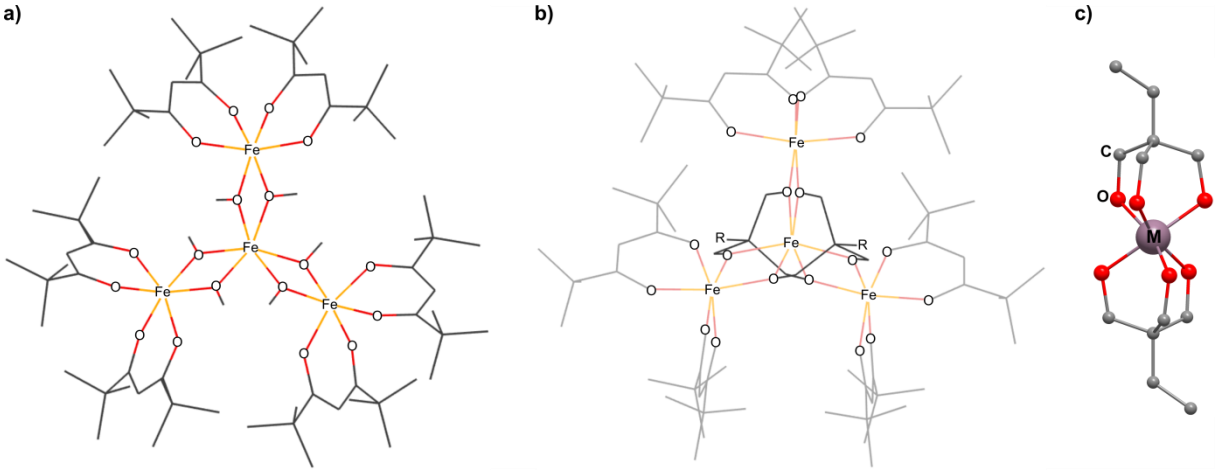

Scheme 1. Representation of the tetranuclear, star-shaped complexes with (a) methoxide and (b) tripodal alkoxide bridges. In (b), the $RC(CH_2O^-)_3$ ligands, here abbreviated $(L^R)^{3-}$, are highlighted in dark grey. (c) Representation of the $M(L^R)_2^{3-}$ "core" (R = Et in this example) formed by the central metal ion and two tripodal anions. The picture in (c) was obtained by removing the peripheral $Fe(dpm)_2^+$ units from the X-ray structure of $[Fe_3Cr(L^{Et})_2(dpm)_6]$, **$Fe_3Cr$** [7].

The parent **Fe_4** complex and its tripodal derivatives were all obtained by "one-pot" self-assembly under N_2 [3, 8]. To increase magnetic anisotropy and rationalize the synthesis of heteronuclear complexes, a modular, three-step approach was successfully developed to synthesize the mixed-metal $[Fe_3Cr(L^R)_2(dpm)_6]$, **Fe_3Cr**, with R = Et, Me or Ph, pure and in high yield [7, 9-11]. The methodology consisted of *(i)* total deprotonation of the tripodal alcohol using Bu^nLi; *(ii)* formation of the $Cr(L^R)_2^{3-}$ core (Scheme 1c); and *(iii)* assembly of the star-shaped complex following the addition of the peripheral $Fe(dpm)_2^+$ units [7]. This modular methodology was also employed for the preparation of a V^{III} derivative $[Fe_3V(L^R)_2(dpm)_6]$, **Fe_3V** (S = 13/2), which presented an anisotropy barrier higher than that of **Fe_4** (20 K *vs* 15 K), a blocking temperature nearly twice as high, and much superior remnant magnetization [10]. Subsequently, the heterometallic gallium(III)/vanadium(III) analog, $[Ga_3V(L^R)_2(dpm)_6]$, **Ga_3V**, was prepared to investigate the origin of the magnetic anisotropy in exchange-coupled systems containing V^{III} [11]. In principle, this modular route could lead to various other metal combinations spanning the central and peripheral positions of the star-shaped framework.

To bring further light onto the molecular assembly mechanism leading to the M_4 complexes, this work started as an effort to synthesize (isolate) the central "core" – the $M^{III}(L^R)_2^{3-}$ moiety (Scheme 1c) that had always been prepared and allowed to react *in situ* during the second and third steps of the synthetic procedure mentioned above [7, 9-11]. Attempts to this synthesis started with M = Ti^{III} and proceeded with the kinetically more stable Cr^{III}; the tripodal alcohols H_3L^R (R = Me, Et or Ph) were initially employed in a 1 M : 2 H_3L^R proportion. The requirement of a deprotonating agent was also investigated.

The reactions gave discrete crystalline products, which, however, did not correspond to a mononuclear structure but to dimeric complexes of general formula $M_2Cl_4(H_2L^R)_2$. Five binuclear compounds with Ti^{III} or Cr^{III} have been prepared, structurally described (see Table S2 for crystallographic information) and characterized by spectroscopic and thermogravimetric techniques. A sixth binuclear product containing titanium(IV), $[Ti_2Cl_4(HL^{Et})_2]$, was obtained after oxidation of the metal ion and further deprotonation of the tripodal ligand.

The crystals were suitable for single-crystal X-ray diffraction (SC-XRD) analysis; all of them contained crystallizing solvent (thf, glyme, MeOH or EtOH) or proligand (H_3L^{Me}) molecules in the unit cell, depending on preparation conditions (Table S2). Tetrahydrofuran was the only solvent consistently lost from the cells, changing the crystal phase and eventually destroying crystallinity. On the other hand, robust intermolecular interaction networks involving the Cr^{III} dimers with cocrystallized alcohols (EtOH and H_3L^R) secured more resistant and easily-handled crystals. The facile formation of the binuclear aggregates and the considerable flexibility of the tripodal scaffold to accommodate chemical changes without loss of structural integrity are discussed.

2. Results and discussion

After comparing more than 20 structures of metal complexes with tripodal ligands in different deprotonation stages, Brechin [12] proposed a relationship between the possible coordination modes of the polyalcohol/alkoxide ligand and

its negative charge. According to the author, when the trialcohol is fully deprotonated, $(L^R)^{3-}$, the oxygen donor atoms usually bind to different metal centers in a variety of coordination ways, reaching saturation in the so-called "3:3:3" mode (first drawing in Scheme 2). When, on the other hand, deprotonation is not complete as in $(HL^R)^{2-}$ and $(H_2L^R)^-$, several other coordination modes, which may involve a smaller number of metal centers, are observed.

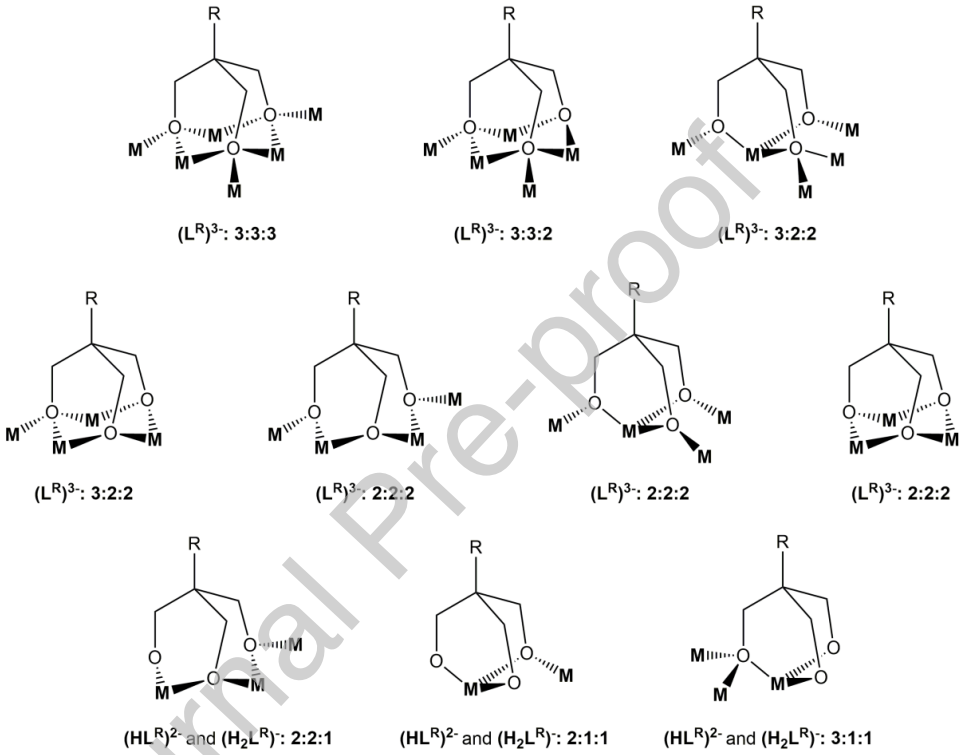

Scheme 2. Representation of different coordination modes for tripodal alcohols/alkoxides adapted from Brechin [12], and sorted according to the degree of deprotonation, $(L^R)^{3-}$, $(HL^R)^{2-}$ and $(H_2L^R)^-$. The numbers below the drawings correspond to the number of metal ions bound to each tripodal oxygen atom.

In the case of the central ("core") unit of the star-shaped complexes that motivated this work (Scheme 1c), each of the two tripodal alkoxides, $(L^R)^{3-}$, chelates the metal centers in a strict 2:2:2 mode; this binding involves one central and three peripheral metal ions (Scheme 2, second row, third structure from the left) [12]. In our quest for isolating the "core", we came across a

symmetric, binucleating 1:2:1 coordination mode (Scheme 3, bottom right) that, although not included in the original Brechin's classification, had an example reported later by the same research group [13].

2.1. Gradual deprotonation studies of H_3L^{Et} using $LiOBu^t$ in the presence of titanium(III)

In a first attempt to synthesize the proposed $M(L^R)_2^{3-}$ core employing M = Ti^{III}, tetrahydrofuran (thf) solutions of the starting material $[TiCl_3(thf)_3]$ and the tripodal ligand H_3L^{Et} received the slow, dropwise addition of different proportions of $LiOBu^t$ (Scheme 3). The lithium alkoxide was employed as deprotonating agent and source of Li^+ to counterbalance the negative alkoxide charge and coordinate to the core. These experiments are detailed below and in the Supplementary Information.

Although several structures similar to the one proposed for the core in Scheme 3 (top right), *i.e.* a central $M(L^R)_2^{3-}$ unit coordinated to three equivalents of Li^+-solvent, have been described [14-20], we did not arrive at the desired product. Instead, a $2H_3L^{Et}$:1Ti:1$LiOBu^t$ proportion led to a dimeric complex, $[Ti_2Cl_4(H_2L^{Et})_2]\cdot 4thf$ (Figure S1, **Ti_2Et**), which was identified by single-crystal X-ray diffraction analysis.

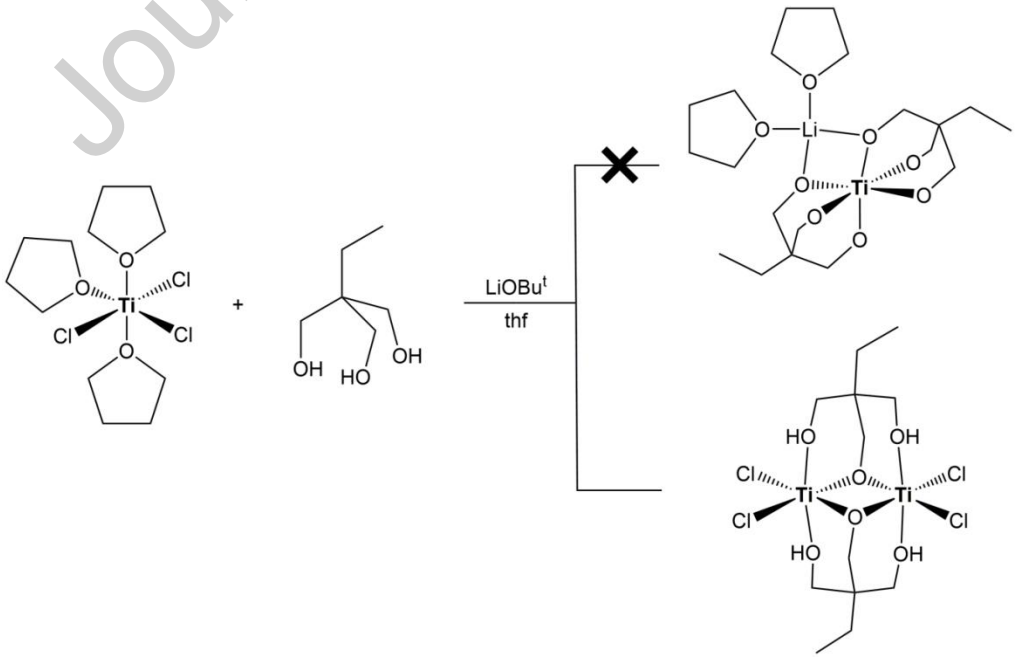

Scheme 3. Attempt to synthesize the $Li_3M^{III}(L^{Et})_2$ "core" by deprotonating the tripodal alcohol. On the top right, a tentative drawing of the desired "core" structure. To simplify the view, only one of the three Li^+ ions coordinated to the oxygen donor atoms of the "core" and solvent molecules has been represented. At the bottom right, the general representation of the dimeric product first obtained with Ti^{III} and later with Cr^{III}, whose structure was solved by X-ray diffraction analysis.

A careful study was then conducted by varying from zero to six the stoichiometric proportion of $LiOBu^t$ to the transition metal ion (see Experimental). Bright green or yellowish-green solutions were respectively obtained when the zero and one base:M^{3+} molar proportions were employed. We later realized that, in both these cases, the green solutions already contained the dimeric type of product that is the main subject of the present report (see Supplementary Information). Brown-reddish solids insoluble in non-protic media were obtained from the reaction mixtures in which the proportion base:H_3L^R was higher than 1:1, and in all cases these powders presented a ligand/metal ratio lower than 2, suggesting the formation of polynuclear aggregates or coordination polymers (Table S1 and discussion that accompanies Figures S1-S3). Several examples in the literature support this aggregation hypothesis [12, 13, 21-26]. Other attempts to isolate the core, changing solvents (to MeOH or glyme), reaction temperature or time, crystallization conditions, or adding diamines as possible terminal ligands for Li^+ did not produce better results (data not shown).

Unexpectedly, the FTIR spectrum of the crystalline solid isolated from the reaction mixture without adding $LiOBu^t$ (compound **P1**, Figure S2) was superposable on that registered for **Ti_2Et**. These results are shown and thoroughly discussed in the Supporting Information. Given this indication that the presence of a deprotonating agent was irrelevant to the preparation of **Ti_2Et**, further syntheses were carried out by the direct (1:1) reaction of the neutral alcohol proligands with different metal starting materials, $[MCl_3(thf)_3]$ (M = Ti^{III}, Cr^{III}) and $CrCl_3 \cdot 6H_2O$, to investigate the generality of the route that led to **Ti_2Et**. At this point, the use of chromium intended to profit from the higher kinetic stability of Cr^{III} coordination compounds compared to those prepared from titanium(III). From then on, the work focused on the reactivity of the different

tripodal alcohols towards Cr^{III}, both in inert atmosphere (N_2) with dry solvents and in air with non-treated solvents, and on the characterization of the dimeric products.

From this point forward, the main products described in this work will be abbreviated as **M_2R** to emphasize their binuclear nature and identify the R group distinguishing the tripodal alcohols. To avoid too elaborated labels, the abbreviation includes the cocrystallized solvent or proligand only when more than one dimer is obtained for the same metal, oxidation state and R group. Table 1 contains the complete set of abbreviations.

Table 1. Binuclear complexes described in this work

Abbreviation	Formulation
Ti_2Et	$[Ti^{III}_2Cl_4(H_2L^{Et})_2]\cdot 4thf$
Ti^{IV}_2Et	$[Ti^{IV}_2Cl_4(HL^{Et})_2]\cdot 2thf$
Cr_2Ph	$[Cr^{III}_2Cl_4(H_2L^{Ph})_2]\cdot 5thf$
Cr_2Me	$[Cr^{III}_2Cl_4(H_2L^{Me})_2]\cdot 2H_3L^{Me}$
Cr_2Et-thf	$[Cr^{III}_2Cl_4(H_2L^{Et})_2]\cdot thf\cdot glyme$
Cr_2Et-EtOH	$[Cr^{III}_2Cl_4(H_2L^{Et})_2]\cdot 2EtOH$

2.2. Syntheses in differing reaction conditions and characterization of the resulting Cr^{III} dimers

The gradual deprotonation approach mentioned above was based on the original synthetic procedure that gave the heterometallic $[Fe_3M'(L^R)_2(dpm)_6]$ complexes by the modular route (M' = Cr^{III}, V^{III} and Ga^{III}), that is, working under inert atmosphere and using non-protic, dry solvents [7]. After isolation from the mother liquor, the **Ti_2Et** dimer could be handled under N_2 but underwent slow degradation over days, even inside Schlenk tubes, visible by the change of color from grayish-green to beige or white. This may relate to a facile loss of crystallizing thf molecules and metal oxidation to titanium(IV) – accompanied by ligand deprotonation – as discussed below.

On the other hand, the chromium(III) analogs **Cr_2Et** and **Cr_2Ph** were resistant to decomposition under similar conditions. Based on this observation and the probable relationship with the low lability of chromium(III) towards substitution reactions [27-29], we decided to explore further the reactivity of this *d*-metal ion towards the tripodal alcohols in conditions very different from those employed in the modular approach. Reactions of $CrCl_3 \cdot 6H_2O$ with H_3L^{Me} or H_3L^{Et} were then carried out in acetonitrile in the air. After workup and recrystallization, $[Cr_2Cl_4(H_2L^{Me})_2] \cdot 2H_3L^{Me}$ (**Cr_2Me**) and $[Cr_2Cl_4(H_2L^{Et})_2] \cdot 2EtOH$ (**Cr_2Et-EtOH**) were isolated in high yield, and their characterization is also described as follows. These findings, taken altogether, suggest that the dimeric species of Cr^{III} described in the present work are thermodynamically stabilized by chelation and hexacoordination to the point in which, even with weak field ligands such as alcohols, alkoxides and halides, they resist redox reactions and hydrolysis.

2.3. Single-crystal X-ray structural analyses (SC-XRD)

All syntheses described in the Experimental Section yielded green crystals mostly suitable for single-crystal XRD analysis (Table S2). The reactions performed in an inert atmosphere using thf as solvent resulted in the rapid crystallization (from minutes to a few hours) of the products from the green mother liquors. The synthesis with Ti^{III} was performed at room temperature, while **Cr_2Et** and **Cr_2Ph** required heating under reflux for 1-2 hours. The procedures in the open air, in turn, gave an opaque green powder that was recrystallized from a thf/ethanol (3:2) mixture, allowing the crystals to form slowly and with good quality.

The overall structure of the dimers, aside from the R groups attached to the tripodal alcohol chain, is quite similar (Figures 1-2 and S4-S5). The coordination environment of the metal ions, Ti^{III} and Cr^{III}, is distorted octahedral, with the M–Cl and $M–O_{alkoxido}$ bonds of the $(H_2L^R)^-$ ligands (of both M centers) lying on the equatorial plane, and two $M–O_{alcohol}$ bonds (of both M centers) in the apical positions. As expected, the bond lengths in the coordination sphere of the metal ions decrease in the order M–Cl > M–O(H)R > M–OR (Table S3). These

dimensions, along with the metal-metal distances, follow the metal ionic radii trend (0.615 Å for Cr^{III} and 0.670 Å for Ti^{III}) [30]. For instance, the non-bonding M···M distance in **Cr_2Et-thf** (average 3.0482(4) Å) is significantly shorter than in **Ti_2Et** (3.1841(6) Å, Table S3).

To the best of our knowledge, only a few previous articles reported binuclear complexes with tripodal bridging ligands as the polyalcohols described in this work; among them, the +III oxidation state for the *d*-block metal is uncommon. One example, containing chromium(III) and 1,1,1-tris(hydroxymethyl)propane (H_2L^{Et}), was obtained from the *in situ* oxidation of a Cr^{II} starting material under reflux in methanol [13]. The other works involve fully-oxidized metal ions such as Ti^{IV}, V^{V}, and W^{VI} [31-33]. As an example, complex $[Ti^{IV}_2Cl_4(HL^{Me})_2]\cdot 2OEt_2$ is structurally analogous to the product **Cr_2Me** introduced herein, except for the oxidation state +IV for the metal accompanied by only one (non-deprotonated) hydroxyl moiety on the tripodal ligand, and diethyl ether as crystallization solvent [32]. Elemental analysis of this compound suggests loss of solvating Et_2O, in line with similar observations made in the present work. Reactions of $(BzPh_3P)[VO_2Cl_2]$ with H_3L^{R} (R = Me, Et, or OH) in methanol, in turn, yielded the also solvated $[(V^{V}O)_2Cl_2(HL^{R})_2]\cdot 2Ph_3BzPCl\cdot 2MeOH$ binuclear complexes [21, 31]. These vanadium(V) compounds differ from most of the dimers produced in this work in the presence of oxido ligands (O^{2-}), only two chlorides, and one protonated arm on each tripodal ligand. Bond lengths and angles in all these reported complexes, taking the different oxidation states into account, are comparable to those observed for the structures herein (Tables S3-S4).

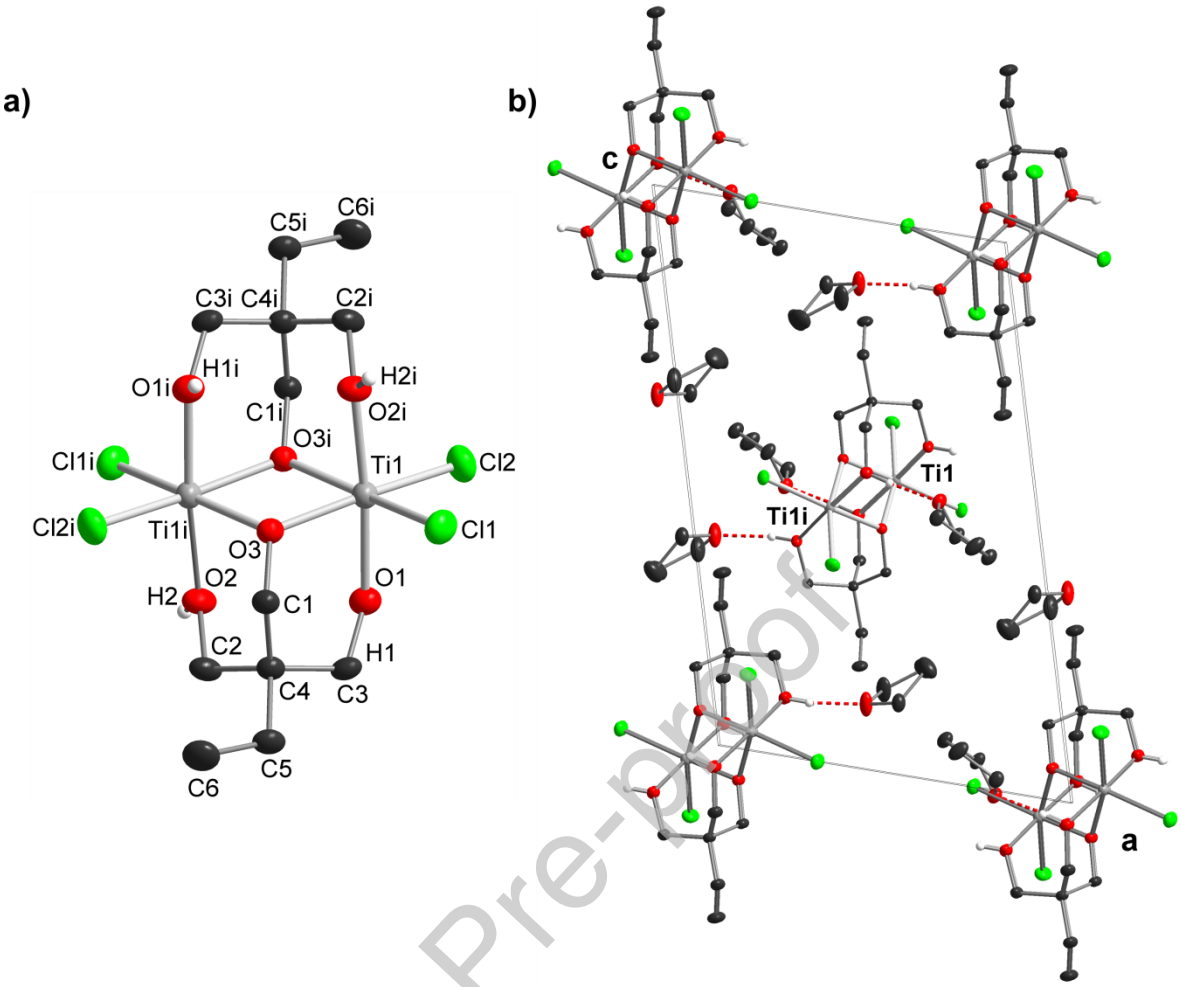

Figure 1. Structural representation of **a)** $[Ti_2Cl_4(H_2L^{Et})_2]$ without solvent molecules; **b)** Unit cell representation of $[Ti_2Cl_4(H_2L^{Et})_2]\cdot 4thf$ (**Ti_2Et**) viewed down the *b* axis. Hydrogen bonds are represented in red. Symmetry code (i): –x+1, –y+1, –z+1.

*2.3.1. Structural details for $[Ti_2Cl_4(H_2L^{Et})_2]\cdot 4thf$ (**Ti_2Et**)* and *$[Ti_2Cl_4(HL^{Et})_2]\cdot 2thf$ (**Ti^{IV}_2Et**)*

Ti_2Et is a titanium(III) complex that crystallizes in the monoclinic system and $P2_1/n$ space group with Z = 2 (Table S2); the asymmetric unit consists of half the dimer and two thf molecules. The only deprotonated arm of the H_2L^{Et} ligand acts as an alkoxide bridge between the two metal centers, whereas the remaining hydroxyl groups each bind a single metal ion and form a hydrogen bond with a neighboring thf molecule. An inversion center located between the metal ions in the dimer builds the whole structure with the unit formula $[M_2Cl_4(H_2L^{Et})_2]\cdot 4thf$ (Figure 1). The complete set of crystallographic data and selected bonds and angles are presented in Tables S2 to S4. The structures of

the two independent molecules of **Cr_2Et-thf**, in turn, are similar to those of **Ti_2Et** and the Cr^{III} dimer prepared by Talbot-Eeckelaers and co-workers [13], differing from the latter in the nature of the cocrystallized solvent molecules (thf and glyme in the case of **Cr_2Et**, and MeOH for the dimer described in the literature). We also note that **Cr_2Et-thf** was obtained directly from a Cr^{III} starting material, while Eeckelaers' complex came from the oxidation of Cr^{II}. This is compatible with a high thermodynamic tendency to form the binuclear framework as it assembles in different reaction media from various starting materials.

In the crystal lattice of **Ti_2Et**, the oxygen atoms of each crystallizing thf molecule are acceptors to rather strong hydrogen bonds with the four remaining hydroxyl groups from the H_2L^{Et} ligands [O(1)–H(1)···O(4) = 1.745(18) Å, 175(4) °, and O(2)–H(2)···O(5) = 1.825(19) Å, 172(4) °] (Table S5). This pattern creates independent $[M_2Cl_4(H_2L^{Et})_2]\cdot 4thf$ units translated along the packing directions. No additional intra- or inter-molecular interaction was observed in the periodic pattern.

After isolation of the **Ti_2Et** crystals, the mother liquor underwent a gradual change from green to blue, violet and then colorless in a matter of days at -20 ^{o}C. Well-formed crystals of acceptable X-ray quality, though in small quantity, were isolated from the final colorless solution and revealed the dimeric structure of **Ti^{IV}_2Et**, $[Ti^{IV}_2Cl_4(HL^{Et})_2]\cdot 2thf$. The product crystallizes in the same space group with similar cell dimensions to those of the Ti^{III} counterpart (Tables S2-S4, Figure 2).

In **Ti^{IV}_2Et**, the oxidation of the metal ions parallels the deprotonation of a second hydroxyl group in each tripodal ligand, keeping the charge balance in the neutral molecule. This oxidation may result from adventitious O_2 introduced by manipulation, but, remarkably, the redox reaction is readily compensated by polyalcohol deprotonation, and the occurrence is reproducible. As a consequence, the dimeric framework of the original **Ti_2Et** product is fully preserved. Structural changes are mainly limited to the effects of the smaller metal radius and number of protonated hydroxyl groups; these, in turn, H-bond

to the only two remaining thf molecules (Figure 2 and packing diagram in Figure S4). The three binding modes for the tripodal ligand are evidenced by clearly different Ti–O bond lengths (Table S3). For the terminal alkoxide group, the Ti–O distance is by far the shortest at 1.7755(8) Å because of the π-donor nature of the RO^- ligand. The average Ti–O bond length in the asymmetric bridge is 2.0247 Å, while the longest metal-oxygen distance (2.1064(8) Å) involves the terminal OH group. Similar dimensions were reported by Nielson and co-workers for a **$Ti^{IV}_2Me{\cdot}2Et_2O$** complex obtained in a small amount from $TiCl_4$ in diethyl ether [32].

Because of the small amount of crystals, **Ti^{IV}_2Et** was characterized only by SC-XRD (Figure 2). The important feature here is the remarkable flexibility of the binuclear skeleton, which accommodates significant chemical changes both to the metal and ligand without decomposition.

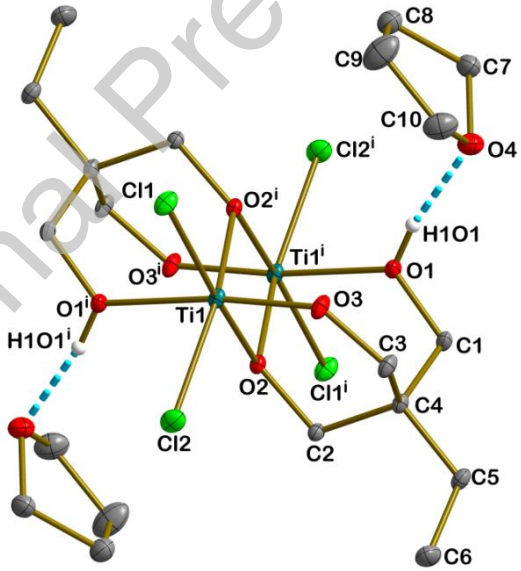

Figure 2. Molecular structure of **Ti^{IV}_2Et**, $[Ti^{IV}_2Cl_4(HL^{Et})_2]{\cdot}2thf$, with the atom numbering scheme. The H-bonds to the thf molecules involve the only two hydroxyl groups (in the asymmetric unit) not deprotonated during complex formation.

2.3.2. Crystal structure descriptions for the chromium(III) dimers

The emerald-green crystals of **Cr_2Ph** were suitable for SC-XRD analysis, notwithstanding their low quality reflected in the high R_{int} value (0.139, Table S2 and Figure S5). The complex crystallizes as very thin needles in the monoclinic system, $P2_1/c$ space group. The asymmetric unit consists of a whole dimer together with five thf molecules, one of which is disordered, rendering a final composition of $[Cr_2Cl_4(H_2L^{Ph})_2]\cdot 5thf$. The unit cell contains four of these asymmetric units (Z = 4), resulting in a cell volume that is 2.5 times larger than that of **Ti_2Et** (Table S2).

In **Cr_2Ph**, four of the five thf molecules are involved in strong hydrogen bonds with the hydroxyl groups of the ligands. One of these four solvent molecules contains one disordered oxygen atom, O(8), which, nonetheless, functions in each site as an acceptor to the strongest H bond in the structure [O(1)–H(1)···O8A = 1.73(5), 159(4) °; O(1)–H(1)···O8B = 1.67(5), 168(4) °, Table S5]. Apart from these interactions, the $[Cr_2Cl_4(H_2L^{Ph})_2]\cdot 5thf$ units are practically isolated in the crystal lattice (Figure S5b). The fifth thf molecule does not participate in any hydrogen bond and therefore can vibrate more freely, displaying a significant level of disorder in two overlapping orientations.

Products **Cr_2Et-thf** and **Cr_2Et-EtOH** crystallize in the triclinic system, $P\bar{1}$ space group (Figure 3a-b). As noted, the molecular structure of **Cr_2Et-thf** is similar to those of **Ti_2Et** and the Cr^{III} dimer prepared by Talbot-Eeckelaers and co-workers [13]. **Cr_2Et-EtOH**, in turn, also consists of a binuclear chromium complex, $[Cr_2Cl_4(H_2L^{Et})_2]$, with two ethanol molecules that complete the crystal packing. **Cr_2Me**, on the other hand, presents $[Cr_2Cl_4(H_2L^{Me})_2]$ cocrystallized with two molecules of H_3L^{Me} (Figure 3c) in the monoclinic system, $P2_1/c$ space group; its asymmetric unit is made up of half a dimer and one H_3L^{Me}.

In **Cr_2Et-thf**, a good hydrogen bond, namely O(4)–H(4)···Cl(1), builds a one-dimensional network connecting the dimers along the [1,1,1] direction and defining a $C_2^2(10)$ (>d<d) motif (Figure 3a, right) [34, 35]. Strong hydrogen bonds also connect the dimers to the thf (H-bond label c) and glyme (H-bond labels a and b) molecules, which alternate as pendant solvents and isolate one

chain from the other. Hydrogen bond dimensions and labels are shown in Table S5.

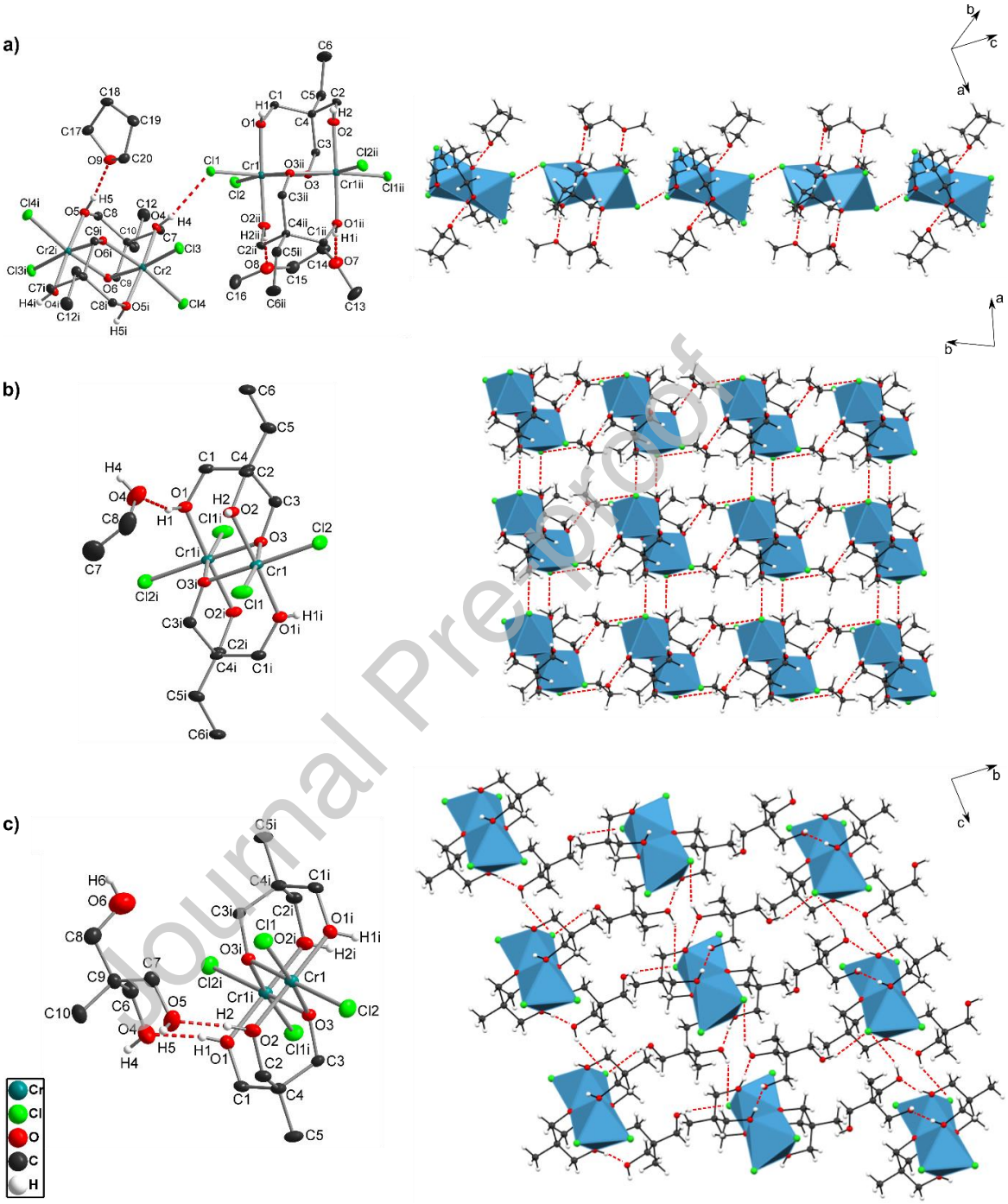

Figure 3. Structural representation of complexes **a)** $[Cr_2Cl_4(H_2L^{Et})_2]\cdot thf\cdot glyme$ (**Cr_2Et-thf**), with two independent molecules linked through good hydrogen bonds; **b)** $[Cr_2Cl_4(H_2L^{Et})_2]\cdot 2EtOH$ (**Cr_2Et-EtOH**) and **c)** $[Cr_2Cl_4(H_2L^{Me})_2]\cdot 2H_3L^{Me}$ (**Cr_2Me**). The figures on the left refer to the ellipsoid representation of each complex displaying the atom numbering schemes. The figures on the right depict the crystal packing of the products, with hydrogen bonds represented as red dashed lines.

For **Cr_2Et-thf**, which contains only ethers as crystallization solvents, the dimeric complexes are almost isolated from one another in the crystal structures. On the other hand, the protic character of the molecules cocrystallized with $[Cr_2Cl_4(H_2L^R)_2]$ in **Cr_2Me** and **Cr_2Et-EtOH** allows them to act as both hydrogen bond donors and acceptors, creating a more complex hydrogen bond network than that discussed above for **Cr_2Et-thf** (Figure 3b-c). This intricate supramolecular networking (see below) probably prevents solvent loss from the **Cr_2Me** and **Cr_2Et-EtOH** crystals and facilitates their handling and analysis, in which they differ strongly from **Cr_2Ph** (see below).

In **Cr_2Et-EtOH**, the hydrogen bonds generate a two-dimensional *ab* sheet in the crystal packing. In this case, the binuclear complexes interact through a strong hydrogen bond, O(2)–H(1O2)···Cl(1), which forms an $R_2^2(8)$ (>b>b) motif with its symmetry-related pair, giving rise to a chain of dimers that extends along the *a* axis (Figures 3b and S6). The *ab* sheet is formed by interaction of the ethanol molecules with two adjacent dimers, giving an $R_4^4(12)$ (>a>d>a>d) motif in the *b* direction (Figure S6). In addition, also along the *b* axis the weak hydrogen bond between a carbon atom from one of the ligand's protonated arms and a chloride atom from another dimer (H-bond label c) connects two adjacent dimer chains in a $R_2^2(10)$ (>c>c) motif (Table S5).

In **Cr_2Me**, in turn, the cocrystallized H_3L^{Me} molecules interact with the protonated arms of the H_2L^{Me} ligands through two strong hydrogen bonds (labels a and b, Figure 3c and Table S5). In this case an $R_4^4(12)$ (>b>f>b>f) motif, along with its symmetry-related equivalents, builds a unidimensional chain along the *c* axis (Figure S7). Additionally, a $C_4^4(22)$ (>b>g<g<b) motif, made up of strong hydrogen bonds and involving both the dimers and the neutral proligand molecules in **Cr_2Me**, gives rise to the two-dimensional web that extends the structure in the [0,1,1] direction (Figure S7). A three-dimensional pattern is then completed by the $C_4^4(22)$ (>b>c<c<b) chain in the [1,0,1] direction, which grows up by alternating the dimers and the cocrystallized H_3L^{Me} molecules (Figure 3c).

2.4. Powder X-ray diffraction (PXRD) analysis

$[Cr_2Cl_4(H_2L^{Ph})_2]\cdot 5thf$ (**Cr_2Ph**) and $[Cr_2Cl_4(H_2L^{Me})_2]\cdot 2H_3L^{Me}$ (**Cr_2Me**), taken as representative of the products cocrystallized with non-protic and protic molecules respectively, have shown an intriguing difference in their PXRD profiles. For the former, a transition from the single-crystal pattern to a second crystalline phase is observed (Figure S8) as the thin needles dry after evaporation of the mother liquor. Such behavior contrasts sharply with the pure single-crystal phase recorded by PXRD for the dry **Cr_2Me** crystals (Figure S9).

As mentioned above, in **Cr_2Ph**, one of the five solvating thf molecules is not involved in H-bonding interactions with any other unit cell component; overall, this is the product that builds the simplest intermolecular interaction network. The loss of this "free" thf molecule is likely responsible for the observed crystalline phase change. For **Cr_2Me**, on the other hand, the cocrystallized tripodal alcohol molecules build an intricate and stabilizing H-bond network involving the dimeric complex (Figure 3c), which limits molecular mobility in the solid-state structure. These findings are supported by the thermogravimetric analysis results (see below).

2.5. Infrared spectroscopy

The infrared spectra of the five M^{III} products are very similar and compatible with alcohol/alkoxide-containing complexes [36-38]. Mostly broad and relatively strong absorptions in the region between 3000 and 3500 cm^{-1} confirm that deprotonation did not occur in all hydroxyl groups. This is in accordance with the structures obtained by single-crystal X-ray diffraction analysis, which shows that terminal O–H groups remain protonated while bridging groups are deprotonated. Spectral comparisons and tentative assignments are presented and discussed in the Supplementary Material (Figures S10-S12 and Tables S6-S8).

2.6. Magnetic susceptibility measurements

Magnetic susceptibility measurements were carried out for the $[Cr_2Cl_4(H_2L^{Ph})_2]\cdot 5thf$ (**Cr_2Ph**) complex. The results show straightforward behavior with an antiferromagnetic coupling manifesting a peak in χ_M and a sharp decrease in $\chi_M T$ values as the temperature is lowered (Figure 4). The $\chi_M T$ *vs* T curve decreases monotonically from 300 to around 50 K, then more sharply at lower temperatures, nearing zero at 2 K. At 300 K, the $\chi_M T$ value is at 3.5 emu K mol^{-1}, against the expected value of 3.75 emu K mol^{-1} for two magnetically isolated *S* = 3/2 centers. The lower experimental value is in agreement with an antiferromagnetic coupling. Curves were fit using the spin Hamiltonian including the isotropic Heisenberg exchange term:

$$\widehat{\mathcal{H}_s} = \mu_B g \hat{\boldsymbol{S}} \vec{B} - 2J \hat{\boldsymbol{S}}_1 \cdot \hat{\boldsymbol{S}}_2$$

The susceptibility and magnetization curves were fit simultaneously and are well-reproduced using the free electron *g*-value, g = 2.0023, and the antiferromagnetic coupling term J = –4.98(1) cm^{-1}.

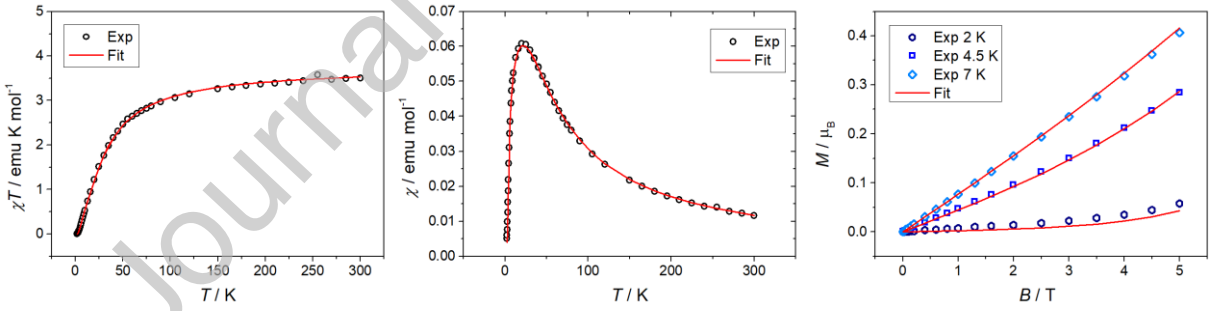

Figure 4. Magnetic susceptibility and magnetization curves for **Cr_2Ph**. The continuous lines correspond to the best fit of the experimental data according to the text.

Quantitative magnetostructural studies of dimeric chromium(III) compounds were first rationalized by Glerup *et al.* in 1983, and their work came to be known as the GHP model [39]. They gathered fifteen chromium hydroxo- or alkoxo-bridged dimers and drew correlations between the exchange coupling constant (*J*) and three structural parameters, the Cr–μ–O bond length (r), the Cr–O–Cr bridging angle (ϕ), and the dihedral angle formed between the R substituents of

the bridging oxygen donors and the Cr_2O_2 plane (θ, see Scheme 4). To illustrate these correlations, comparative structural and magnetic data for several chromium alkoxo-bridged dimers can be found in Table 2.

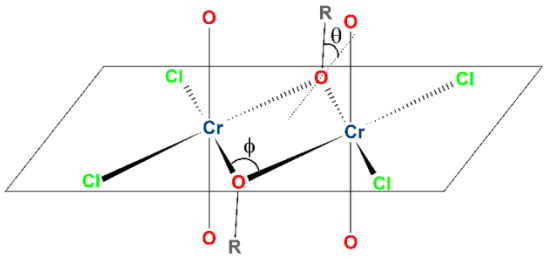

Scheme 4. Schematic representation of the structure of the **Cr_2Ph** dimer illustrating relevant structural parameters, namely the angles ϕ (Cr–O–Cr) and θ (R –O–Cr–O). In this drawing, the dihedral angle ψ, related to the planarity of the Cr_2O_2 ring (see text), equals zero.

In the report by Talbot-Eeckelaers and co-workers, which described the structure analogous to **Cr_2Et-thf** and **Cr_2Et-EtOH** with methanol as a crystallization solvent, a detailed study of the molecule's magnetic behavior was presented [13]. The complex showed antiferromagnetic coupling between the chromium ions, in agreement with the GHP model's prediction. Theoretical calculations at the DFT level were carried out for a model complex, $[Cr_2(\mu\text{-}OMe)_2(H_2O)_2Cl_4]$, to investigate the impact of the ϕ bridging angle on the exchange coupling *J*. The authors found that a variation in *J* was not linear with the bridging angle, with the coupling remaining antiferromagnetic in the whole ϕ range observed (80-120^o). Despite this finding, at around the angle found for most of the alkoxo-bridged chromium dimers described in the literature (*ca*. 101^o; Table 2), the antiferromagnetic coupling constant is the closest to zero. According to the authors, at low angles the Cr···Cr distance becomes too short, favoring direct exchange mechanisms which strongly reinforce the antiferromagnetic contributions to the exchange coupling. On the other hand, in complexes in which the ϕ angle is much larger – such as those with bulkier ligands – the alkyl groups of the alkoxide bridges tend to be almost coplanar with the Cr_2O_2 ring. This trend also strengthens the antiferromagnetic character of the interaction.

A more recent report by Fraser and coworkers [40] expanded on the existing correlations. Studying structural variations in a model compound at the DFT level through the broken symmetry approach, the authors found a linear correlation between the coupling constant *J* and the dihedral angle θ, with higher tilts of the R group associated with a stronger ferromagnetic contribution, and the turning point between ferromagnetic and antiferromagnetic coupling at θ = 47.3°. However, the authors also found that θ alone was insufficient to describe the magnetic behavior of these dimeric complexes – the planarity of the Cr_2O_2 ring (referred to as angle ψ, the Cr–O–Cr–O dihedral angle) also played an important role in modulating the overall magnetic interaction. Highly planar rings tend to favor antiferromagnetic exchange due to the overlap between the d orbitals of the chromium centers and the p orbitals of the bridging oxygens [39, 40]. Thus, only by considering both factors can a meaningful prediction be made about the nature of the exchange coupling. In their expanded model, the original turning point between ferro- and antiferromagnetic exchange (θ = 47.3°) only produces ferromagnetic interaction if ψ is about 2.8°.

This correlation may well justify the scarcity of ferromagnetically-coupled chromium(III) complexes found in the literature, and a more recent work by the same authors has further demonstrated the importance of the ψ angle by analyzing the ferromagnetic exchange in a series of complexes with non-planar Cr_2O_2 rings [41]. By synthesizing several chromium dimers with two bridging alkoxide groups and one additional bridging carboxylate moiety, the authors added an extra exchange pathway and bent the alkoxide-bridged Cr_2O_2 ring by up to 20°, resulting in eight ferromagnetically-coupled dimers.

The structural and magnetic data of the **Cr_2Ph** complex described here agree with the more common trends established by previous literature (Table 2). The dihedral angle θ is around 45°, and the Cr–O–Cr–O torsion angle ψ is 0.07°, both of which point to weak antiferromagnetic coupling. Terminal chloride ligands are not expected to impose significant changes on the exchange interaction. As can be observed from Table 2, complexes with wildly different terminally-coordinated ligands (such as chloride, acetylacetonate (acac), 3-Cl-

acac, 3-Br-acac, pyridine or water) all present comparable exchange coupling constant values. The more significant changes are only introduced when the nature or spatial disposition of the bridging ligands is varied.

It is interesting to remark that, for the most part, binuclear chromium(III) alkoxides present bridges that are either monodentate or part of a ligand backbone that is not particularly rigid. Fraser's 2017 paper, in particular, features two bidentate alkoxides as bridging ligands (2-hydroxymethylpyridine – hmpH, and 2-hydroxyethylpyridine – hepH, see Table 2) [40]. The longer hydroxyethyl arm of the hep ligand allows for greater structural flexibility, leading to a much smaller tilt of the R group concerning the Cr_2O_2 ring. As a result, the antiferromagnetic coupling in the hep complex is significantly enhanced. Conversely, it should be expected that a more rigid ligand backbone might have the opposite effect.

In this context, the structure of the tripodal ligands in **Cr_2Ph** (and also **Cr_2Et-thf**, **Cr_2Et-EtOH** and **Cr_2Me**) does not impose significant structural rigidity. The tripodal alcohol coordinates with some distortion on the ligand structure itself, with the bond angles between the quaternary carbon atom and the methylene arms falling into the 110.15-111.84^o range for the **Cr_2Ph** molecule. Comparatively, the crystal structure of the free tripodal alcohol presents those angles in the 107.3-109.1^o range [42]. This lack of rigidity is unsurprising given the aliphatic, acyclic nature of the ligand, and it translates into a good accommodation of the tripodal alcohol into the fairly regular octahedral coordination environment found in the complexes presented in this paper. Additionally, there is no tension in the coordination framework to break the planarity of the Cr_2O_2 ring. Thus, no deviation from the general case of weak antiferromagnetic coupling would be expected. This observation also suggests that, despite the chelating nature of the bridging ligands in **Cr_2Ph**, models considering only monodentate bridging alkoxide groups (as in the Talbot-Eeckelaers and Fraser's DFT studies) can make reliable predictions of magnetic coupling [13, 40].

Table 2. Structural and magnetic coupling data for several alkoxo-bridged chromium(III) dimers

Compound	Cr–O_{bridge} (Å)	Cr–O–Cr (ϕ)	θ (°)[a]	ψ (°)[a]	J (cm^{-1})[b]	Ref.
[{Cr(H_2L^{Ph})Cl_2(μ-OMe)}$_2$] (**Cr_2Ph**)	1.960-1.988	101.14; 100.76	44.64-44.15	0.07	–4.87	This work
[{Cr(H_2L^{Et})Cl_2(μ-OMe)}$_2$]	1.955-1.964	100.91	44.32; 44.54	0	–6.15	[13]
[{Cr(acac)$_2$(μ-OMe)}$_2$]	1.950-1.973	101.29; 100.76	36.05-38.15	1.37	–4.9	[43]
[{Cr(3-Cl-acac)$_2$(μ-OMe)}$_2$]	1.959	101.09	30.31; 30.6	0	–4.91	[44]
[{Cr(3-Br-acac)$_2$(μ-OMe)}$_2$]	1.961-1.963	101.44	31.53; 31.79	0	–4.27	[45]
[{Cr(3-Br-acac)$_2$(μ-OEt)}$_2$]	1.949-1.953	101.75	22.85; 23.53	0	–8.94	[45]
[{Cr(pic)$_2$(μ-OMe)}$_2$][c]	1.951-1.970	100.67; 101.76	21.13; 23.45	0.91	–14.13	[40]
[{Cr(H_2O)Cl_2(μ-hmp)}$_2$][c]	1.943-1.969	101.50; 101.61	17.70; 23.78	0	–5.77	[40]
[{Cr(H_2O)Cl_2(μ-hep)}$_2$][c]	1.943-1.963	102.99	7.00	0	–9.35	[40]
[{$CrCl_2$(py)(μ-hmp)}$_2$][c]	1.967-2.000	100.63; 100.65	48.84; 55.44	1.55 4.90	–6.16	[40]

a – Dihedral angles defined in Scheme 4. b – Using the -2J(S_1·S_2) formalism where 2J corresponds to the singlet-triplet splitting.
c – pic = picolinate; hmpH = hydroxymethylpyridine; hepH = hydroxyethylpyridine.

2.7. Thermogravimetric analysis

The easy loss of crystallization solvent during manipulation and under ordinary storage conditions appeared to be a common feature among the solvated compounds prepared from tetrahydrofuran, which differ, in this respect, from those synthesized in more polar media and recrystallized from ethanol-containing mixtures. This loss is first manifested by comparing the expected (from SC-XRD results) and observed carbon and hydrogen percentages, as shown in the Experimental section.

To better characterize this apparent solvent mobility in the solid state, thermal analyses were conducted for **Cr_2Ph**, **Cr_2Me** and **Cr_2Et-EtOH**. For **Cr_2Ph**, the thermogravimetric (TG) profile and the corresponding derivative thermogravimetry (DTG) curve show at least three major stages of weight loss (Figure 5a), with the broad nature of the DTG peaks evidencing the existence of overlapping thermal events. The number of events in the first step (up to 130 °C, 14.5 wt%) is not well-resolved in the DTG profile. The weight change is compatible with the loss of two solvating tetrahydrofuran molecules (calculated at 14.9%), supporting the hypothesis of easy solvent displacement from the crystalline solid. Then follows the second step (*ca.* 130-200 °C), also related to

the loss of thf (third molecule; exp. 7.7%; calc. 7.4%). From this point on, displacement of the two remaining solvent molecules and an H_2L^{Ph} ligand determines the third step (200-400 °C; exp. 32.2% *vs* calculated 33.6%). The additional mass loss, measured up to 900 °C (*ca.* 16%), is attributed to the final H_2L^{Ph} decomposition; the difference from the calculated value (18.7%) is probably due to the final setup temperature. It is worth noting that the tripodal ligands are only displaced above 200 °C, supporting their relevant stabilizing role. The solid residue at 900 °C corresponds to 29.8% of the initial sample mass and probably consists of chromium oxides and chlorides.

Remarkably, although the thf molecules in the crystal lattice of **Cr_2Ph** are not covalently bound to the dimeric framework, some of them are lost at a relatively high temperature (130-400 ^{o}C, as noted above). This reflects the quite strong hydrogen bonds that fix them in the crystal (section 2.3.2 and Table S5). On the other hand, according to the DTG profile in Figure 5a, the most pronounced mass loss in the first thermal event occurs at around 75-85 °C, which could be due to the highly disordered thf molecule in the crystal structure of **Cr_2Ph**. This agrees with the fact that this unique thf molecule does not interact with any other unit cell component through hydrogen bonds (see the structural discussion in section 2.3.2).

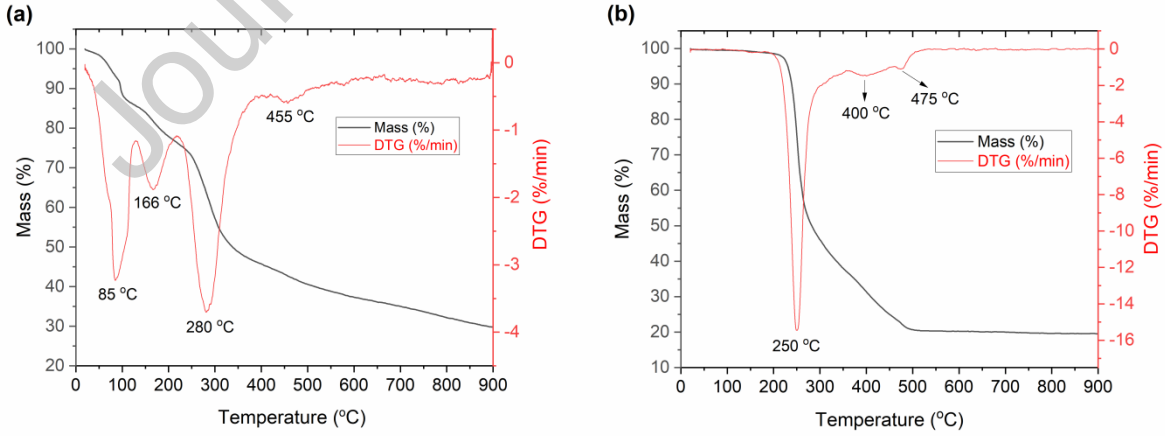

Figure 5. Thermogravimetric (TG) and derivative thermogravimetry (DTG) curves registered at 10 °C min^{-1} for (a) $[Cr_2Cl_4(H_2L^{Ph})_2]\cdot 5thf$ (**Cr_2Ph**) and (b) $[Cr_2Cl_4(H_2L^{Me})_2]\cdot 2H_3L^{Me}$ (**Cr_2Me**) with N_2 as carrier gas.

To confirm the solvent loss indicated by elemental and thermogravimetric analyses, a freshly-prepared batch of crystalline **Cr_2Ph** was weighed before and after being kept under vacuum (10^{-3}/10^{-4} Torr) for 24 h at room temperature. The observed weight loss (measured 14.9%) agrees very well with the first step in the TG curve (exp. 14.5 wt%, Figure 5a). This again indicates the high mobility of at least some of the solvating thf molecules in the crystalline packing.

TG and DTG analyses of **Cr_2Me** and **Cr_2Et-EtOH** confirm that the complexes containing cocrystallized alcohol molecules (H_3L^{Me} and EtOH, respectively), which form robust H-bond networks in the crystals, are more resistant to thermal decomposition. In both cases, there is no significant weight loss below 150 ^{o}C (200 ^{o}C for **Cr_2Me**; Figures 5b and S13), which is in striking contrast with the data for **Cr_2Ph** (Figure 5a). For **Cr_2Me**, the mass loss event up to 280 ^{o}C, evidenced by the sharp DTG peak at 250 ^{o}C, corresponds to the removal of the two cocrystallized H_3L^{Me} molecules and one H_2L^{Me} ligand (exp. 49.4%; calc. 49.6%). The second tripodal ligand is lost up to 360 ^{o}C (13.8 *vs* 14.4%). **Cr_2Et-EtOH**, in turn, loses the cocrystallized ethanol molecules and both H_2L^{Et} ligands in two main thermal events up to 360 ^{o}C (exp. 55.8%; calc. 59.3%). In all cases, the tripodal ligands are lost above 200 ^{o}C, but the smaller and less H-bonded cocrystallized solvents, thf and EtOH, particularly the former, are lost earlier. For both **Cr_2Me** and **Cr_2Et-EtOH**, the thermal events above 350 ^{o}C appear to be related to the loss of chloride, and the final solid residue corresponds to *ca.* 20% of the initial sample mass.

3. Experimental

3.1. General

Most syntheses and analyses, except those involving **Cr_2Et-EtOH** and **Cr_2Me**, were performed using an inert nitrogen atmosphere (99.999%, Praxair) and Schlenk or glove-box techniques. The solvents (Honeywell/Riedel de Haen, Aldrich, Vetec) were purified by standard methods [46], dried and distilled immediately before use. Reagents $[MCl_3(thf)_3]$ (wherein M = Cr or Ti) were

prepared according to the literature [47-49]. The tripodal alcohol 1,1,1-tris(hydroxymethyl)phenylmethane (H_3L^{Ph}) was synthesized following the method by Viguier [50]. The alcohol 1,1,1-tris(hydroxymethyl)propane (H_3L^{Et}), in turn, was acquired from Aldrich and recrystallized from toluene/thf 1:1 at -20 ^{o}C. The other reagents were also provided by Sigma-Aldrich and used without purification. **Cr_2Et-EtOH** and **Cr_2Me** were synthesized and recrystallized in the air using non-treated solvents.

3.2. Instrumentation

Elemental analyses were performed by MEDAC Laboratory in Chobham (Surrey, England) or by the Analytical Center of the University of São Paulo (Brazil) on a Thermal Scientific Flash ES 1112 Series or a PerkinElmer 2400 Series II elemental analyzer, respectively. Fourier-transform infrared (FTIR) absorption spectra in the region of 4000 to 400 cm^{-1} were recorded using a BOMEM MB or a Varian FTIR-640 spectrophotometer. Air-sensitive samples were prepared as emulsions with mineral oil (Nujol) under N_2 and spread between two KBr plates. The oil was dried with sodium metal before use. Spectra of air-stable samples were recorded from KBr pellets. Electronic spectra were obtained in aqueous solutions from a Varian Cary 50 spectrophotometer in the region of 350–800 nm (Figures S14 and S15). Thermogravimetric (TG) data were collected on a Netzsch STA449 F3 Jupiter thermal analyzer equipped with a silicon carbide furnace and using dinitrogen as carrier gas. A weighed portion (*ca*. 4 mg) of each sample was heated in an aluminum pan at 10 °C min^{-1} from 20 to 900 °C.

Powder X-ray diffraction profiles (Cu-Kα radiation, λ = 1.5406 Å) were measured from samples packed in Hilgenberg glass capillaries (0.5 mm diameter, glass no. 14). Bruker D8 Discovery equipment with a rotating capillary Debye-Scherrer setup was employed; measurements were performed at room temperature. Diffraction data were collected from 5° to 50° 2θ in 0.01° steps over 72 h. The powder pattern was analyzed with TOPAS v.5 developed by Bruker AXS Corporation [51].

Single-crystal X-ray diffraction data were collected on a Bruker D8 Venture diffractometer equipped with a Photon 100 CMOS detector, Mo-Kα and Cu-Kα radiation sources and a graphite monochromator. Mo-Kα radiation was used for **Ti^{IV}_2Et**, **Cr_2Me**, and **Cr_2Et-EtOH**; Cu-Kα for **Ti_2Et**, **Cr_2Ph**, and **Cr_2Et-thf**. Data were processed using the APEX2 program for **Ti_2Et**, and APEX3 for the remaining compounds [52, 53]. The structure of **Cr_2Et-EtOH** was determined by the direct methods routines in the SHELXS program [54], while those for **Ti^{IV}_2Et**, **Cr_2Me**, **Ti_2Et**, **Cr_2Ph**, and **Cr_2Et-thf** employed intrinsic phasing routines in the SHELXT software [55, 56]. In all cases, refinement was carried out by full-matrix least-squares methods in SHELXL [57, 58]. Scattering factors for neutral atoms were taken from the literature [59]. Computer programs used in this analysis have been noted above and were run through WinGX [60, 61]. Drawings were made with the Diamond 4 and Mercury software [62, 63].

3.3. Magnetic measurements

Direct current (dc) magnetic measurements were performed on a Superconducting Quantum Interference Device (SQUID) magnetometer with a 5 T superconductive magnet. For the experiment, 10.7 mg of polycrystalline **Cr_2Ph** were ground in the glove-box and enveloped in Teflon to obtain a pellet. The temperature dependence of the magnetization was measured under a constant magnetic field of 10 kOe from 300 to 30 K and 1 kOe from 30 K to 2 K. The magnetization as a function of the magnetic field was measured at 2.0, 4.5 and 7.0 K. The experimental data were corrected for the diamagnetic contributions of the sample and Teflon using Pascal constants [64]. All the experimental curves were fit simultaneously using the PHI analysis software [65].

3.3. Syntheses

3.3.1. Gradual deprotonation studies of H_3L^{Et} using $LiOBu^t$ in the presence of titanium(III)

A light blue solution of $[TiCl_3(thf)_3]$ (*ca.* 0.50 g, 1.3 mmol) in thf (50 mL) was added dropwise to a colorless H_3L^{Et} solution (ca. 0.37 g, 2.7 mmol) in thf (30 mL) over 3 h, leading to a clean, bright green solution. This order of addition was chosen to allow better visualization of color changes in the reaction mixtures. In these assays, a 1:2 metal-to-ligand molar ratio was always employed. Varying amounts of $LiOBu^t$ (0, 1, 2, 3, or 6 molar equivalents per mol of M^{3+}) were solubilized in thf (30 mL), and the resulting colorless solution was then slowly added to the previous system over approximately 2 h. The final color of the mixture depended on the amount of $LiOBu^t$ added (Supporting Information). Out of the five reaction conditions employed, only the ones using $LiOBu^t$: Ti^{3+} 0:1 and 1:1 proportions gave green crystals, of which those obtained from the 1:2:1 mixture ($[TiCl_3(thf)_3]$: H_3L^{Et} : $LiOBu^t$) were suitable for single-crystal X-ray diffraction analysis (**Ti_2Et**, Figure S1). These crystals were poorly soluble in thf and soluble in methanol, producing very light green and light yellow solutions, respectively. The yellow color suggests reaction with the solvent. The other products were reddish-brown or orange-brown powders that dissolved only in methanol (thf, glyme, hexane, and toluene were also tested), producing light yellow solutions. These powders were analyzed by FTIR, as shown in Figures S2 and S3.

3.3.2. General procedure for reactions between Ti^{III} and Cr^{III} starting materials and H_3L^{Et} and H_3L^{Ph} in an inert atmosphere

Suspensions of $[MCl_3(thf)_3]$, M = Ti^{III} (0.371 g) or Cr^{III} (0.375 g), 1.0 mmol, in 60 mL of thf (or a mixture of 1 thf : 2 glyme in the case of **Cr_2Et-thf**) received the addition of solid H_3L^R, R = Ph (0.182 g) or Et (0.134 g), 1.0 mmol, under stirring at room temperature. This procedure gave clear solutions whose shade of green depended on each metal/ligand combination. The crystalline products formed quickly at room temperature, except for **Ti_2Et**, which required cooling at -20 °C for a few days. In the syntheses involving chromium(III), the reaction mixtures were heated to 50-70 ^oC for 1-2 hours while changing from lilac to

pinkish-green; crystals formed on cooling to room temperature. All solids were isolated by filtration and quickly dried under vacuum or N_2 flow.

Despite the proportions of crystallizing solvent revealed by SC-XRD analysis, the products prepared in thf gave different elemental composition results depending on the time of storage and handling conditions of the distinct samples, implying differing thf contents. These solids became opaque after prolonged vacuum drying or long storage under N_2. The experimental contents of carbon and hydrogen were employed to fit the formulations reported as follows.

$[Ti_2Cl_4(H_2L^{Et})_2]\cdot 4thf$ (**Ti_2Et**): grayish-green crystals (0.120 g, 30.3% yield). Elemental analysis calculated for $[Ti_2Cl_4(H_2L^{Et})_2]\cdot 1.5thf$ ($C_{18}H_{38}Cl_4O_{7.5}Ti_2$): C 35.21; H 6.24. Found: C 35.84; H 6.86. Repeating this analysis in another batch of crystals revealed again a proportion between 1.5 and two molecules of crystallizing thf per dimeric molecule.

$[Cr_2Cl_4(H_2L^{Ph})_2]\cdot 5thf$ (**Cr_2Ph**): emerald green, small needles (0.309 g, 63.8% yield). Elemental analysis calculated for $[Cr_2Cl_4(H_2L^{Ph})_2]\cdot 2thf$ ($C_{28}H_{42}Cl_4Cr_2O_8$): C 44.70; H 5.63. Found: C 44.79; H 5.60.

$[Cr_2Cl_4(H_2L^{Et})_2]\cdot thf\cdot glyme$ (**Cr_2Et-thf**): green, small needles (0.0822 g, 24.4% yield). This complex crystallized from a 1:2 thf/glyme (dimethoxyethane) mixture. Elemental analysis calculated for $[Cr_2Cl_4(H_2L^{Et})_2]\cdot glyme$ ($C_{16}H_{36}Cl_4Cr_2O_8$): C 31.91; H 6.02. Found: C 31.58; H 6.33. Of the two solvents observed in the unit cell (thf and glyme), these results suggest a loss of tetrahydrofuran.

3.3.4. Synthesis of Cr^{III} dimers with H_3L^{Me} and H_3L^{Et} in acetonitrile

The direct reaction between the proligand H_3L^{Me} (0.501 g, 4.17 mmol) and $CrCl_3\cdot 6H_2O$ (0.555 g, 2.08 mmol) in acetonitrile (20 mL) was carried out in the air. The reaction mixture was stirred at 80 °C for 24 h, forming a dark green

suspension. The solid product was isolated by filtration and recrystallized from thf/ethanol (3:2), giving dark green crystals after three days under vapor diffusion with diethyl ether. The synthetic procedure employed with H_3L^{Et} (0.503 g, 3.75 mmol) was similar, in which the proligand was stirred with $CrCl_3 \cdot 6H_2O$ (0.496 g, 1.86 mmol) under reflux at 80 °C for 24 h, followed by recrystallization from thf/ethanol/Et_2O.

$[Cr_2Cl_4(H_2L^{Me})_2] \cdot 2H_3L^{Me}$ (**Cr_2Me**): green crystals soluble in water and polar organic solvents (0.654 g, 86.8% yield). Elemental analysis calculated for $C_{20}H_{46}O_{12}Cl_4Cr_2$: C 33.13; H 6.35; Cr 14.36%. Found: C 33.10; H 6.40; Cr 14.91%.

$[Cr_2Cl_4(H_2L^{Et})_2] \cdot 2EtOH$ (**Cr_2Et-EtOH**): green crystals soluble in water and polar organic solvents (0.462 g, 82.2% yield). Elemental analysis calculated for $C_{16}H_{38}O_8Cl_4Cr_2$: C 31.70; H 6.65; Cr 17.15%. Found: C 31.63; H 6.67; Cr 16.88%.

4. Conclusions

In the light of our attempts to isolate the "$Li_3M'(L^R)_2$ core" (Schemes 1c and 3), either by gradual deprotonation of the polyalcohols or use of chelating ligands with high affinity for Li^+ (to prevent polynuclear aggregation), the stabilization of that particular "core" in the star-shaped M_4 complexes apparently demands the coordination of the peripheral ions provided by the $Fe(dpm)_2^+$ synthon [2, 3, 7, 10]. The replacement of Li^+ in "$Li_3M'(L^R)_2$" with $Fe(dpm)_2^+$ is probably driven by the higher affinity of the transition metal ion for the core, as compared to Li^+, leading to the spontaneous self-assembly of the tetranuclear architecture. In the absence of the peripheral synthons, as described in this work, the discrete mononuclear "core" cannot be prepared.

Tripodal H_3L^R alcohols provide a highly versatile coordination environment for early transition metal(III)/(IV) ions such as those investigated in this work. The chelating and yet flexible binding of the tridentate polyalcohol stabilizes the

molecular framework, while their ability to readily deprotonate compensates for redox changes suffered by the metal. It is a "win-win" situation in which the hydroxyl groups in the "alcohol mode" are amenable to coordination to M^{III} while the efficient π-donor alkoxide derivatives suit well the +IV oxidation state. In this scenario, metal oxidation such as that giving **Ti^{IV}_2Et**, for example, does not lead to product decomposition as in several other ligand environments of early transition M^{III} ions. Instead, a new crystalline M^{IV} dimer is cleanly formed and is structurally analogous to the M^{III} counterpart. An additional investigation on other metal(III/IV) redox pairs is desirable; it would inform if titanium(III)/(IV) is a unique combination and what experimental conditions favor such a neat redox transformation.

In these complexes, the versatile binuclear skeleton accommodates *intramolecular* chemical changes while its polar groups establish *intermolecular* networks with neighboring molecules in the solid state. In this regard, tetrahydrofuran is a weakly interacting partner as compared to alcohols; other ethers are described to behave similarly in analogous complexes. The easy displacement of the solvating ether molecules from the unit cell is an interesting feature regarding possible structural consequences. On the other hand, solvating alcohol molecules such as ethanol or H_3L^R form (with the dimers) more complex and robust supramolecular arrangements that are resistant to the loss of crystallinity.

Differently from the products crystallized from thf, **Cr_2Me** and **Cr_2Et-EtOH** are soluble (without reaction) in water and short chain alcohols. Considering this solubility, the coordinating ability of the ligands, their structural flexibility, and the robustness of the dimeric framework – which forms and maintains integrity in very distinct experimental environments – the products described herein present a reasonable potential to act as precursors to more complex homo and heteronuclear architectures, given proper reaction conditions.

Acknowledgements

Authors are grateful to Brazilian CNPq [Conselho Nacional de Desenvolvimento Científico e Tecnológico, grants 308426/2016-9 and 314581/2020-0], CAPES [Coordenação de Aperfeiçoamento de Pessoal de Nível Superior, Finance Code 001] and PrInt/CAPES-UFPR Internationalization Program for scholarships and financial support. This work has also been supported by Italian MIUR [Project PRIN 2015-HYFSRT and Progetto Dipartimenti di Eccellenza 2018–2022, ref B96C1700020008]. We are very grateful to the technical staff from the Department of Chemistry/UFPR and Department of Chemistry and Biology/UTFPR, particularly Dr. Rubia Camila R. Bottini and Mr. Angelo Roberto dos Santos Oliveira, for performing the metal and thermogravimetric analyses. The access to the LAMAQ/UTFPR (Multi-User Laboratory of Chemical Analysis) is also appreciated.

Supplementary materials

FTIR spectra and assignment tables, packing diagrams, hydrogen bond parameters, powder X-ray diffraction and thermogravimetric profiles, and electronic spectra are presented as Electronic Supplementary Material. Complete crystallographic data sets for all complexes have been deposited with the Cambridge Crystallographic Data Centre under the CCDC numbers 2201210 (**Ti_2Et**), 2201211 (**Ti^{IV}_2Et**), 2201212 (**Cr_2Ph**), 2201213 (**Cr_2Me**), 2201214 (**Cr_2Et-thf**), and 2201215 (**Cr_2Et-EtOH**). These data can be obtained free of charge via http://www.ccdc.cam.ac.uk/conts/retrieving.html (or from the Cambridge Crystallographic Data Centre, 12, Union Road, Cambridge CB2 1EZ, UK; fax: +44 1223 336033). Supplementary material associated with this article can be found, in the online version, at doi: XXXXXXXXX.

References

[1] A.L. Barra, A. Caneschi, A. Cornia, F. Fabrizi de Biani, D. Gatteschi, C. Sangregorio, R. Sessoli, L. Sorace, Single-Molecule Magnet Behavior of a Tetranuclear Iron(III) Complex. The Origin of Slow Magnetic Relaxation in Iron(III) Clusters, J. Am. Chem. Soc. 121(22) (1999) 5302-5310.

[2] A. Cornia, A.C. Fabretti, P. Garrisi, C. Mortalò, D. Bonacchi, D. Gatteschi, R. Sessoli, L. Sorace, W. Wernsdorfer, A.-L. Barra, Energy-Barrier Enhancement by Ligand Substitution in Tetrairon(III) Single-Molecule Magnets, Angew. Chem. Int. Ed. 43(9) (2004) 1136-1139.

[3] S. Accorsi, A.-L. Barra, A. Caneschi, G. Chastanet, A. Cornia, A.C. Fabretti, D. Gatteschi, C. Mortalò, E. Olivieri, F. Parenti, P. Rosa, R. Sessoli, L. Sorace, W. Wernsdorfer, L. Zobbi, Tuning Anisotropy Barriers in a Family of Tetrairon(III) Single-Molecule Magnets with an S = 5 Ground State, J. Am. Chem. Soc. 128(14) (2006) 4742-4755.
[4] A. Cornia, L. Gregoli, C. Danieli, A. Caneschi, R. Sessoli, L. Sorace, A.-L. Barra, W. Wernsdorfer, Slow quantum relaxation in a tetrairon(III) single-molecule magnet, Inorg. Chim. Acta 361(12) (2008) 3481-3488.
[5] M. Mannini, F. Pineider, C. Danieli, F. Totti, L. Sorace, P. Sainctavit, M.A. Arrio, E. Otero, L. Joly, J.C. Cezar, A. Cornia, R. Sessoli, Quantum tunnelling of the magnetization in a monolayer of oriented single-molecule magnets, Nature 468(7322) (2010) 417-421.
[6] L. Poggini, E. Tancini, C. Danieli, A.L. Sorrentino, G. Serrano, A. Lunghi, L. Malavolti, G. Cucinotta, A.L. Barra, A. Juhin, M.A. Arrio, W.B. Li, E. Otero, P. Ohresser, L. Joly, J.P. Kappler, F. Totti, P. Sainctavit, A. Caneschi, R. Sessoli, A. Cornia, M. Mannini, Engineering Chemisorption of Fe-4 Single-Molecule Magnets on Gold, Advanced Materials Interfaces 8(24) (2021).
[7] P. Totaro, K.C.M. Westrup, M.-E. Boulon, G.G. Nunes, D.F. Back, A. Barison, S. Ciattini, M. Mannini, L. Sorace, J.F. Soares, A. Cornia, R. Sessoli, A new approach to the synthesis of heteronuclear propeller-like single molecule magnets, Dalton Trans. 42(13) (2013) 4416-4426.
[8] E. Tancini, M.J. Rodriguez-Douton, L. Sorace, A.-L. Barra, R. Sessoli, A. Cornia, Slow Magnetic Relaxation from Hard-Axis Metal Ions in Tetranuclear Single-Molecule Magnets, Chem. Eur. J. 16(34) (2010) 10482-10493.
[9] L. Sorace, M.E. Boulon, P. Totaro, A. Cornia, J. Fernandes-Soares, R. Sessoli, Origin and spectroscopic determination of trigonal anisotropy in a heteronuclear single-molecule magnet, Phys. Rev. B 88(10) (2013) 104407.
[10] K.C.M. Westrup, M.-E. Boulon, P. Totaro, G.G. Nunes, D.F. Back, A. Barison, M. Jackson, C. Paulsen, D. Gatteschi, L. Sorace, A. Cornia, J.F. Soares, R. Sessoli, Adding Remnant Magnetization and Anisotropic Exchange to Propeller-like Single-Molecule Magnets through Chemical Design, Chem. Eur. J. 20(42) (2014) 13681-13691.
[11] K.C.M. Westrup, F.S. Santana, D.L. Hughes, G.G. Nunes, J.F. Soares, A.-L. Barra, R. Sessoli, L. Sorace, The Intricate Determination of Magnetic Anisotropy in Quasi-octahedral Vanadium(III): An HF-EPR and Magnetic Study, Appl. Magn. Reson. 51(11) (2020) 1233-1250.
[12] E.K. Brechin, Using tripodal alcohols to build high-spin molecules and single-molecule magnets, Chem. Commun. (41) (2005) 5141-5153.
[13] C.E. Talbot-Eeckelaers, G. Rajaraman, J. Cano, G. Aromí, E. Ruiz, E.K. Brechin, Encouraging Chromium(III) Ions to Form Larger Clusters: Syntheses, Structures, Magnetic Properties and Theoretical Studies of Di- and Octametallic Cr Clusters, Eur. J. Inorg. Chem. 2006(17) (2006) 3382-3392.
[14] J.I. Davies, J.F. Gibson, A.C. Skapski, G. Wilkinson, W. Wai-Kwok, Synthesis of the hexaphenoxotungstate(V) ion; The X-ray crystal structures of the tetraethylammonium and lithium salts, Polyhedron 1(7) (1982) 641-646.
[15] W.C.A. Wilisch, M.J. Scott, W.H. Armstrong, Vanadium(III) phenolate complexes. Synthesis, structure, and properties of $[\{V(OC_6H_5)_6\}\{Li(DME)\}_3]$ and two species containing the $[V(DIPP)_4]$- anion (DME = 1,2-dimethoxyethane, DIPP = 2,6-diisopropylphenolate), Inorg. Chem. 27(24) (1988) 4333-4335.
[16] U. Piarulli, D.N. Williams, C. Floriani, G. Gervasio, D. Viterbo, Carbohydrate metal complexes as ligands for alkali cations, J. Chem. Soc., Chem. Commun. (12) (1994) 1409-1410.
[17] U. Piarulli, A.J. Rogers, C. Floriani, G. Gervasio, D. Viterbo, Metallohosts Derived from the Assembly of Sugars around Transition Metals: The Complexation of Alkali Metal Cations, Inorg. Chem. 36(26) (1997) 6127-6133.
[18] R.J. Cross, L.J. Farrugia, D.R. McArthur, R.D. Peacock, D.S.C. Taylor, Syntheses, Crystal Structures, and CD Spectra of Simple Heterobimetallic Transition Metal Binaphtholates, Inorg. Chem. 38(25) (1999) 5698-5702.
[19] H. Ikeda, T. Monoi, Y. Nakayama, H. Yasuda, Synthesis and structure of a chromium(III) complex coordinated by 1,1′-Bi-2-naphtholate ligands and its catalytic activity for ethylene polymerization, J. Organomet. Chem. 648(1) (2002) 226-230.

[20] A.J. Wooten, P.J. Carroll, P.J. Walsh, Insight into Substrate Binding in Shibasaki's $Li_3(THF)_n(BINOLate)_3Ln$ Complexes and Implications in Catalysis, J. Am. Chem. Soc. 130(23) (2008) 7407-7419.

[21] Y. Chang, Q. Chen, M.I. Khan, J. Salta, J. Zubieta, Coordination chemistry of the tetrametalate core, $\{M_4O_{16}\}$: syntheses from $[V_2O_2Cl_2\{(OCH_2)_2C(R)(CH_2OH)\}_2]$ and structures of the mixed-metal cluster $[V_2Mo_2O_8(OMe)_2\{(OCH_2)_3CR\}_2]_2$- and the reduced cluster $[V_4O_4(H_2O)_2(SO_4)_2\{(OCH_2)_3CR\}_2]_2$, J. Chem. Soc., Chem. Commun. (24) (1993) 1872-1874.

[22] D.C. Crans, F. Jiang, J. Chen, O.P. Anderson, M.M. Miller, Syntheses, X-ray Structures, and Solution Properties of $[V_4O_4\{(OCH_2)_3CCH_3\}_3(OC_2H_5)_3]$ and $[V_4O_4\{(OCH_2)_3CCH_3\}_2(OCH_3)_6]$: Examples of New Ligand Coordination Modes, Inorg. Chem. 36(6) (1997) 1038-1047.

[23] G. Rajaraman, M. Murugesu, E.C. Sañudo, M. Soler, W. Wernsdorfer, M. Helliwell, C. Muryn, J. Raftery, S.J. Teat, G. Christou, E.K. Brechin, A Family of Manganese Rods: Syntheses, Structures, and Magnetic Properties, J. Am. Chem. Soc. 126(47) (2004) 15445-15457.

[24] C.J. Milios, M. Manoli, G. Rajaraman, A. Mishra, L.E. Budd, F. White, S. Parsons, W. Wernsdorfer, G. Christou, E.K. Brechin, A Family of $[Mn_6]$ Complexes Featuring Tripodal Ligands, Inorg. Chem. 45(17) (2006) 6782-6793.

[25] L.F. Jones, D.M. Low, M. Helliwell, J. Raftery, D. Collison, G. Aromí, J. Cano, T. Mallah, W. Wernsdorfer, E.K. Brechin, E.J.L. McInnes, Fe(III) clusters built with tripodal alcohol ligands, Polyhedron 25(2) (2006) 325-333.

[26] I.S. Tidmarsh, E. Scales, P.R. Brearley, J. Wolowska, L. Sorace, A. Caneschi, R.H. Laye, E.J.L. McInnes, Synthesis, Structural, and Magnetic Studies on a Redox Family of Tetrametallic Vanadium Clusters: $\{V^{IV}_4\}$, $\{V^{III}_2V^{IV}_2\}$, and $\{V^{III}_4\}$ Butterfly Complexes, Inorg. Chem. 46(23) (2007) 9743-9753.

[27] R. van Eldik, Inorganic High Pressure Chemistry: Kinetics and Mechanisms, Elsevier, Amsterdam, 1986.

[28] C.H. Langford, H.B. Gray, Ligand Substitution Processes, W. A. Benjamin, New York, 1965.

[29] R.B. Jordan, Reaction Mechanisms of Inorganic and Organometallic Systems, 2nd ed., Oxford University Press, New York, 1998.

[30] R.D. Shannon, Revised effective ionic radii and systematic studies of interatomic distances in halides and chalcogenides, Acta Crystallogr. Sect. A 32(5) (1976) 751-767.

[31] J. Salta, J. Zubieta, Oxovanadium alkoxide complexes. Syntheses and crystal structures of $(Ph_4P)_2[(VO)_2Cl_4(OR)_2]$ (R = $-CH_3$, $-CH_2CH_2Cl$) and $[(VO)_2Cl_2MeC(CH_2OH)(CH_2O)_{22}]$, Inorg. Chim. Acta 257(1) (1997) 83-88.

[32] A.J. Nielson, C. Shen, J.M. Waters, Bis(μ-2-hy-droxy-methyl-2-methyl-propane-1,3-diolato)bis-[di-chlorido-titanium(IV)] diethyl ether disolvate, Acta Crystallogr Sect E Struct Rep Online 69(Pt 12) (2013) m676-m677.

[33] R. Delmont, A. Proust, F. Robert, P. Herson, P. Gouzerh, The building block approach to the synthesis of polyoxotrisalkoxometalates, Comptes Rendus de l'Académie des Sciences - Series IIC - Chemistry 3(2) (2000) 147-155.

[34] J. Bernstein, R.E. Davis, L. Shimoni, N.-L. Chang, Patterns in Hydrogen Bonding: Functionality and Graph Set Analysis in Crystals, Angewandte Chemie International Edition in English 34(15) (1995) 1555-1573.

[35] D.S. Hughes, A. Delori, A. Rehman, W. Jones, Using crystallography, topology and graph set analysis for the description of the hydrogen bond network of triamterene: a rational approach to solid form selection, Chem. Cent. J. 11(1) (2017) 63.

[36] K. Nakamoto, Infrared and Raman Spectra of Inorganic and Coordination Compounds, 5th ed., Wiley-Interscience, New York, 1997.

[37] K. Nakamoto, Infrared and Raman Spectra of Inorganic and Coordination Compounds Part B, 6th ed., New Jersey, 1996.

[38] N.Y. Turova, E.P. Turevskaya, V.G. Kessler, M.I. Yanovskaya, The Chemistry of Metal Alkoxides, Springer, New York, 2002.

[39] J. Glerup, D.J. Hodgson, E. Pedersen, A Novel Correlation between Magnetism and Structural Parameters in Superexchange Coupled Chromium(III) Dimers, Acta Chem. Scand. 37a (1983) 161-164.

[40] H.W.L. Fraser, G.S. Nichol, G. Velmurugan, G. Rajaraman, E.K. Brechin, Magneto-structural correlations in a family of di-alkoxo bridged chromium dimers, Dalton Trans. 46(22) (2017) 7159-7168.
[41] H.W.L. Fraser, L. Smythe, S. Dey, G.S. Nichol, S. Piligkos, G. Rajaraman, E.K. Brechin, A simple methodology for constructing ferromagnetically coupled Cr(iii) compounds, Dalton Trans. 47(24) (2018) 8100-8109.
[42] R. Winpenny, D. Henderson, A. Parkin, S. Parsons, D. Messenger, CCDC 278247: Experimental Crystal Structure Determination, CSD Communication, Cambridge, UK, 2005.
[43] H.R. Fischer, J. Glerup, D.J. Hodgson, E. Pedersen, Structural and magnetic characterization of the alkoxo-bridged chromium(III) dimer bis(μ-methoxo)bis[bis(2,4-pentanedionato)chromium(III)], $[(acac)_2Cr(OCH_3)]_2$, Inorg. Chem. 21(8) (1982) 3063-3066.
[44] E.D. Estes, R.P. Scaringe, W.E. Hatfield, D.J. Hodgson, Synthesis and structural and magnetic characterization of the alkoxo-bridged chromium(III) dimer di-μ-methoxo-bis[bis(3-chloro-2,4-pentanedionato)chromium(III)], Inorg. Chem. 15(5) (1976) 1179-1182.
[45] E.D. Estes, R.P. Scaringe, W.E. Hatfield, D.J. Hodgson, Structural and magnetic characterization of the alkoxo-bridged chromium(III) dimers di-μ-methoxy-bis[bis(3-bromo-2,4-pentanedionato)-chromium(III)] and di-μ-ethoxy-bis[bis(3-bromo-2,4-pentanedionato)chromium(III)], Inorg. Chem. 16(7) (1977) 1605-1610.
[46] D.D. Perrin, W.L. Armarego, Purification of Laboratory Chemicals, 3rd ed., Butterworth-Heinemann, Oxford, 1997.
[47] W. Herwig, H. Zeiss, Notes: Chromium Trichloride Tetrahydrofuranate, The Journal of Organic Chemistry 23(9) (1958) 1404-1404.
[48] R.J.H. Clark, J. Lewis, D.J. Machin, R.S. Nyholm, 59. Complexes of titanium trichloride, Journal of the Chemical Society (Resumed) (1963) 379-387.
[49] L.E. Manzer, Tetrahydrofuran complexes of selected early transition-metals, Inorg. Synth. 21 (1982) 135-140.
[50] R. Viguier, G. Serratrice, A. Dupraz, C. Dupuy, New Polypodal Polycarboxylic Ligands − Complexation of Rare-Earth Ions in Aqueous Solution, Eur. J. Inorg. Chem. 2001(7) (2001) 1789-1795.
[51] A.A. Coelho, TOPAS and TOPAS-Academic: an optimization program integrating computer algebra and crystallographic objects written in C++, J. Appl. Crystallogr. 51(1) (2018) 210-218.
[52] Bruker, APEX3, SAINT and SADABS software, Bruker AXS Inc., Madison, Wisconsin, USA, 2016.
[53] Bruker, APEX2 software, Bruker AXS, Madison, Wisconsin, USA, 2014.
[54] G.M. Sheldrick, SHELXS – Programs for crystal structure determination (SHELXS-2013) University of Göttingen, Germany, 2013.
[55] G.M. Sheldrick, SHELXT - Integrated space-group and crystal-structure determination, Acta Crystallogr. Sect. A 71(1) (2015) 3-8.
[56] G. Sheldrick, A short history of SHELX, Acta Crystallographica, Section A: Foundations and Advances 64(1) (2008) 112-122.
[57] G.M. Sheldrick, SHELXL – Programs for crystal structure refinement (SHELXL-2014), University of Göttingen, Germany, 2014.
[58] G.M. Sheldrick, Crystal structure refinement with SHELXL, Acta Crystallogr. Sec. C: Struct. Chem. 71 (2015) 3-8.
[59] A.J.C. Wilson, International Tables for X-ray Crystallography, Kluwer Academic Publishers, Dordrecht 1992.
[60] L.J. Farrugia, WinGX suite for small-molecule single-crystal crystallography, J. Appl. Crystallogr. 32(4) (1999) 837-838.
[61] L.J. Farrugia, WinGX and ORTEP for Windows: an update, J. Appl. Crystallogr. 45 (2012) 849-854.
[62] K. Brandenburg, DIAMOND, Crystal Impact GbR, Bonn, Germany, 2006.
[63] C.F. Macrae, I. Sovago, S.J. Cottrell, P.T. Galek, P. McCabe, E. Pidcock, M. Platings, G.P. Shields, J.S. Stevens, M. Towler, Mercury 4.0: from visualization to analysis, design and prediction, J. Appl. Crystallogr. 53(1) (2020) 226-235.
[64] G.A. Bain, J.F. Berry, Diamagnetic Corrections and Pascal's Constants, J. Chem. Educ. 85(4) (2008) 532-536.

[65] N.F. Chilton, R.P. Anderson, L.D. Turner, A. Soncini, K.S. Murray, PHI: A powerful new program for the analysis of anisotropic monomeric and exchange-coupled polynuclear d- and f-block complexes, J. Comput. Chem. 34(13) (2013) 1164-1175.

Carla Krupczak, Bruno J. Stoeberl, Kátia C. M. Westrup

Investigation, Methodology, Validation, Writing - Original Draft

Lorenzo Tesi

Investigation, Validation, Writing - Review & Editing

Francielli S. Santana

Investigation, Methodology, Validation, Writing - Review & Editing

Siddhartha O. K. Giese

Investigation, Validation, Writing - Original Draft

Fabiano Yokaichiya, Daniel da S. Costa

Investigation, Methodology, Validation, Writing - Review & Editing

Juliana M. Missina

Writing - Original Draft, Writing - Review & Editing, Visualization

Danilo Stinghen

Investigation, Writing - Review & Editing

David L. Hughes

Validation, Supervision, Writing - Review & Editing

Roberta Sessoli

Validation, Supervision, Writing - Review & Editing, Project administration, Funding acquisition

Giovana G. Nunes

Investigation, Methodology, Validation, Supervision, Writing - Review & Editing

Dayane M. Reis

Conceptualization, Methodology, Supervision, Writing - Review & Editing, Project administration, Funding acquisition

Jaísa F. Soares

Conceptualization, Methodology, Supervision, Writing - Review & Editing, Project administration, Funding acquisition

Declaration of interests

☒The authors declare that they have no known competing financial interests or personal relationships that could have appeared to influence the work reported in this paper.

☐The authors declare the following financial interests/personal relationships which may be considered as potential competing interests: